Computers, Materials & Continua CMC, vol.63, no.1, pp.41-64, 2020

Agglomeration Effects on Static Stability Analysis of Multi-Scale Hybrid Nanocomposite Plates

Farzad Ebrahimi[1], Ali Dabbagh[2], Abbas Rastgoo[2] and Timon Rabczuk[3, *]

Abstract: We propose a multiscale approach to study the influence of carbon nanotubes' agglomeration on the stability of hybrid nanocomposite plates. The hybrid nanocomposite consists of both macro- and nano-scale reinforcing fibers dispersed in a polymer matrix. The equivalent material properties are calculated by coupling the Eshelby-Mori-Tanaka model with the rule of mixture accounting for effects of CNTs inside the generated clusters. Furthermore, an energy based approach is implemented to obtain the governing equations of the problem utilizing a refined higher-order plate theorem. Subsequently, the derived equations are solved by Galerkin's analytical method to predict the critical buckling load. The influence of various boundary conditions is studied as well. After validation, a set of numerical examples are presented to explain how each variant can affect the plate's natural frequency.

Keywords: Buckling, agglomeration, multi-scale hybrid nanocomposites, Eshelby-Mori-Tanaka model.

1 Introduction

Laminated composites are fabricated by inserting each ply with a desirable orientation angle to achieve pre-defined mechanical properties. Due to their remarkable characteristics, such composites have gained the attention in the engineering community. In the early 2000s, Zenkour et al. [Zenkour and Fares (2001)] presented a general mechanical analysis on the laminated composite shells independent from any additional shear correction coefficient. Static and dynamic answers of laminated plates via a meshless method are explored by Wang et al. [Wang, Liew, Tan et al. (2002)] with respect to various edge conditions of the structure. Patel et al. [Patel, Ganapathi and Makhecha (2002)] used a finite element method (FEM) to estimate the hygro-thermo-elastic buckling and free vibration behaviors of laminated composite plate via a C^0 continuous element. Later, Ferreira et al. [Ferreira and Carrera (2005)] developed a grid-free approximation function to probe the free vibration problem of a laminated plate in

[1] Department of Mechanical Engineering, Faculty of Engineering, Imam Khomeini International University, Noroozian Blvd., Qazvin, Iran.

[2] School of Mechanical Engineering, College of Engineering, University of Tehran, Tehran, Iran.

[3] Institute of Research and Development, Duy Tan University, Da Nang, Vietnam.

[*] Corresponding Author: T. Rabczuk. Email: timon.rabczuk@uni-weimar.de.

Received: 14 July 2019; Accepted: 13 August 2019.

the framework of Mindlin's plate theory. Aydogdu [Aydogdu (2007)] studied the thermo-elastic stability limits of multi-layered composite beams employing a higher-order beam theorem. Chai et al. [Chai and Yap (2008)] developed a closed form FE model to derive the lateral modulus of laminated composite beams and showed its applicability in static and dynamic problems of Euler-Bernoulli beams. Another study has been performed by Ćetković et al. [Ćetković and Vuksanović (2009)] to present a layerwise displacement field for mechanical behaviors of laminates. Putting emphasize on the crucial role of choosing a proper shape function in higher-order theories, [Aydogdu (2009)] introduced a new shear deformable model for laminated composite plates and showed its application in the cases of vibration, bending and buckling problems. Carrera's unified formulation (CUF) has been utilized by Fazzolari et al. [Fazzolari and Carrera (2011)] solving the vibration and stability problems of laminated composite plates on the basis of various approximation techniques. CUF has again been used together with a zig-zag kinematic theorem and a finite difference approach in order to study both static and dynamic answers of composite plates [Rodrigues, Roque, Ferreira et al. (2011)]. Other authors exploited isogeometric analysis (IGA) for the mechanical response of laminated elements [Thai, Ferreira, Bordas et al. (2014); Yu, Yin, Bui et al. (2016)].

Another popular composite commonly used in designs is the fiber reinforced composite (FRC). In this type, the desirable properties can be generated by inserting a group of fibers such as glass- or carbon-fibers into a matrix with a designed orientation angle. Aref et al. [Aref and Alampalli (2001)] studied fiber reinforced polymers (FRPs) including the vibrational mode shapes of bridges consisting of FRPs. Tita et al. [Tita, Ferreira, Bordas et al. (2003)] examined the dynamic behaviors of FRC beams both experimentally and theoretically. Zenkour [Zenkour (2004)] performed a viscoelastic stability analysis of FRC plates using both classical and higher-order plate theories. A genetic algorithm (GA) based model has been proposed by Roy et al. [Roy and Chakraborty (2009)] to optimize the vibration control of FRP shells. In another research, Mareishi et al. [Mareishi, Rafiee, He et al. (2014)] investigated the electro-mechanical nonlinear mechanical static and dynamic behaviors of fiber reinforced piezoelectric beams. [Sepahvand (2016)] carried out a FEM based stochastic dynamic study on FRCs.

Once elements with at least one dimension in nano scale are selected as reinforcements, the composite is named a nanocomposite. One of the most famous nano-sized reinforcements are carbon nanotubes (CNTs). Numerous researchers have investigated the static and dynamic behavior of CNT reinforced (CNTR) nanocomposites. For example, Ke et al. [Ke, Yang and Kitipornchai (2010)] utilized Timoshenko beam model incorporated with von Kármán relations to study the nonlinear vibrational behavior of CNTR nanocomposite beams. In another attempt, [Zhu, Lei and Lieu (2012)] employed Mindlin plate theory coupled with FEM to study the static and dynamic responses of CNTR nanocomposite plates. Shen et al. [Shen and Xiang (2014)] investigated the thermo-elastic postbuckling problem of a cylindrical CNTR nanocomposite panel. Heshmati et al. [Heshmati, Yas and Daneshmand (2015)] predicted the dynamic characteristics of a CNTR beam and studied the influence of CNTs' agglomeration and waviness. Lei et al. [Lei, Zhang and Liew (2015)] utilized a kp-Ritz method in order to study the vibration analysis of nanocomposite plates reinforced with single-walled CNTs (SWCNTs) in the framework of Mindlin plate theory. Wattanasakulpong et al.

[Wattanasakulpong and Chaikittiratana (2015)] presented an efficient model for bending, buckling and vibration behaviors of CNTR nanocomposite plates based on a higher-order plate model. Jam et al. [Jam and Kiani (2015)] presented a solution for low-velocity impact problem of a nanocomposite beam while the structure is subjected by thermal loading. An Isogeometric analysis (IGA) in conducted by Phung-Van et al. [Phung-Van, Abdel-Wahab, Liew et al. (2015)] for both stability and vibration problems of CNTR nanocomposite plates on the basis of Reddy's plate model. Song et al. [Song, Zhang and Liew (2016)] employed a higher-order plate theory to consider impact responses of CNTR nanocomposite structures with respect to different distributions of CNTs in the initial matrix. Lei et al. [Lei, Zhang and Liew (2016)] developed a parametric study for dynamic behaviors of rotating cylindrical panels reinforced with CNTs on the basis of an element free kp-Ritz method. The low-velocity impact analysis of nanocomposite plates in thermal environments has been carried out by Ebrahimi et al. [Ebrahimi and Habibi (2017)]. An Eshelby-Mori-Tanaka based homogenization model for CNTR nanocomposite panels is developed by García-Macías et al. [García-Macías, Rodríguez-Tembleque, Castro-Triguero et al. (2017)] investigating the postbuckling characteristics of such structures under axial compression with respect to waviness and agglomeration effects. Ebrahimi et al. [Ebrahimi and Farazmandnia (2018)] examined the thermally affected mechanical responses of sandwich beams made of CNTR nanocomposites.

However, CNTs are not the only nano size reinforcement which is used in nanocomposites. Graphene platelets (GPLs) have been recently employed by researchers to design and analyze novel nanocomposites. Song et al. [Song, Kitipornchai and Yang (2017)] investigated both free and forced vibrational characteristics of GPL reinforced (GPLR) plates. García-Macías et al. [García-Macías, Rodriguez-Tembleque and Sáez (2018)] surveyed the frequency and deflection characteristics of nanocomposite plates reinforced with both graphene and CNT. Song et al. [Song, Yang and Kitipornchai (2018)] highlighted the effects of GPLs as reinforcements in the bending and buckling responses of nanocomposite plates on the basis of Mindlin plate theory.

Also popular are so-called hybrid nanocomposites, which are made of three phases: a matrix, macro-scale reinforcements and nano-scale reinforcements. These hybrid nanocomposites empowers the structure to support higher critical stability limit, natural frequency and also lower deflections. Several studies on the mechanical responses of such hybrid nanocomposites have been conducted. Rafiee et al. [Rafiee, Liu, He et al. (2014)] surveyed the nonlinear dynamic characteristics of piezoelectric laminated plates. He et al. [He, Rafiee, Mareishi et al. (2015)] explored the large amplitude nonlinear free and forced vibrational responses of multi-scale hybrid nanocomposite beams. Later, Rafiee et al. [Rafiee, Nitzsche and Labrosse (2016)] investigated the static and dynamic responses of thin-walled rotating hybrid nanocomposite beams. Ghorbanpour Arani et al. [Ghorbanpour Arani, BabaAkbar Zarei, Eskandari et al. (2017)] studied the vibrational responses of double-layered sandwich beams made from a smart core and facesheets made from multi-scale hybrid CNT/glass fiber reinforced nanocomposites. Ebrahimi et al. [Ebrahimi and Habibi (2018)] determined the behavior of hybrid nanocomposite plates in a hygrothermal environment when the structure is subjected to a low-velocity impactor. They considered kinematical nonlinearities on the basis of von-Karman theory. The presented paper is focused on an analytical study of the buckling characteristics of multi-scale hybrid

nanocomposite plates. Therefore, a blend of Eshelby-Mori-Tanaka micromechanical model and rule of mixture is implemented to homogenize the material. Afterwards, a refined plate theory is extended and the equations of motion are derived based on the dynamic form of the principle of virtual work. Next, Galerkin's method is used to solve the governing equations and the influence of several imput parameters is studied.

2 Theory and formulation

2.1 Problem definition

As shown in Fig. 1, the length and width of the plate are presumed to be *a* and *b*, respectively; the thickness of the structure is assumed to be *h*. It is worth mentioning that the structure is reinforced with a mixture of multi-scale reinforcing gadgets. In this research, carbon based reinforcements are employed, (CFs) and CNTs in particular.

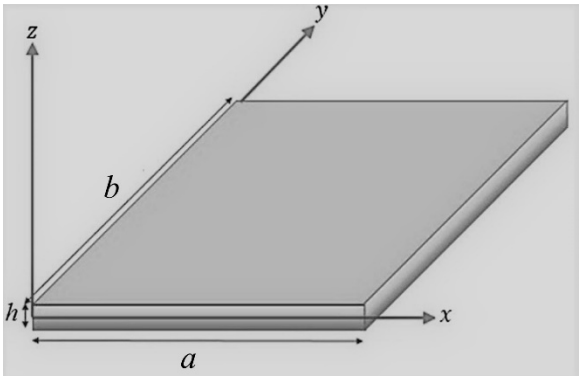

Figure 1: Geometry of a rectangular plate

2.2 Micromechanical homogenization scheme

In this section, the homogenization process is explained presenting a Eshelby-Mori-Tanaka model in order to capture the effect of CNTs' agglomeration while reaching the effective mechanical properties of multi-scale hybrid nanocomposites Shi et al. [Shi, Feng, Huang et al. (2004)]. Furthermore, the rule of mixture is employed in order to account for the dispersion of CFs in the nanocomposite. First, the effective properties of CF reinforced (CFR) composites are going to be discussed as follows:

$$E_{11} = V_F E_{11}^F + V_{NCM} E^{NCM} \tag{1}$$

$$\frac{1}{E_{22}} = \frac{1}{E_{22}^F} + \frac{V_{NCM}}{E^{NCM}} - V_F V_{NCM} - \frac{\frac{\left(\nu^F\right)^2 E^{NCM}}{E_{22}^F} + \frac{\left(\nu^{NCM}\right)^2 E_{22}^F}{E^{NCM}} - 2\nu^F \nu^{NCM}}{V_F E_{22}^F + V_{NCM} E^{NCM}} \tag{2}$$

$$\frac{1}{G_{12}} = \frac{V_F}{G_{12}^F} + \frac{V_{NCM}}{G^{NCM}} \tag{3}$$

$$\rho = V_F \rho^F + V_{NCM} \rho^{NCM} \tag{4}$$

$$\nu_{12} = V_F \nu^F + V_{NCM} \nu^{NMC} \tag{5}$$

where E, G, ν and ρ stand for Young's modulus, shear modulus, Poisson's ratio and mass density, respectively. Also, the superscripts F and NCM denote fiber and nanocomposite matrix, respectively. Evidently, V_F and V_{NCM} are volume fractions of fiber and nanocomposite matrix, respectively. Obviously, the aforementioned volume fractions can be related to each other by:

$$V_F + V_{NCM} = 1 \tag{6}$$

Next, we investigate the effect of adding nanoparticles to the media. CNTs, which are employed as the nano scale reinforcements in this article, possess a remarkable stiffness incorporated with a high slenderness ratio. Due to these features, sometimes CNTs do not follow the initial uniform distribution inside the matrix. In other words, in some regions inside the continua some spherical inclusions can be found which are filled with a set of CNTs. Thus, CNTs' concentration can be different from a region to another one. This effect is of high significance whenever the mechanical behavior of a nanocomposite is supposed to be analyzed. in this situation, the total volume of CNTs can be divided in two parts, one of them is related to the CNTs inside the inclusions and another one corresponds with CNTs which are inserted in the matrix. The volume of CNTs inside the inclusions (clusters) W_r^{in} and the volume of CNTs inside the matrix W_r^M can be related to each other as:

$$W_r = W_r^{in} + W_r^M \tag{7}$$

Now, it is turned to relate the volume of CNTs to the entire volume of the structure as follows:

$$W = W_r + W_M \tag{8}$$

where W_M is the volume of the matrix which CNTs are dispersed in it. In this paper, a polymeric matrix is utilized. Also, W_r is the volume of CNTs. Dividing these volumes to the total volume (W), the volume fraction of each part can be written as:

$$V_r = \frac{W_r}{W}, \qquad V_M = \frac{W_M}{W} \tag{9}$$

As same as the volume of CNTs (W), the volume fraction of CNTs in the matrix can be divided in two parts of inside the clusters and outside of clusters. To this reason, two new parameters are introduced to formulate this issue in the following form:

$$\mu = \frac{W_{in}}{W}, \qquad \eta = \frac{W_r^{in}}{W_r} \tag{10}$$

where μ indicates on the volume fraction of clusters and η stands for the volume fraction of CNTs inside the clusters. It should be regarded that $\mu \leq \eta$ is a limitation for this methodology. One should be aware of the particular cases which can be generated by changing agglomeration parameters. For instance, once μ=1, the entire matrix can be considered as a big cluster which contains all of the nanoparticles, henceforward,

aggregation of nanofillers cannot be observed. However, full accumulation can occur in the situation that η=1 (fully agglomerated CNTs). In another condition ($\mu \leq \eta$, $\eta \neq 1$), some of the nanofillers are placed inside the clusters and the others are scattered in the matrix free from any membrane (partially agglomerated CNTs).

Now, incorporating the Eqs. (9) and (10) yields in:

$$\frac{W_r^{in}}{W_{in}} = \frac{V_r \eta}{\mu} \tag{11}$$

$$\frac{W_r^{M}}{W - W_{in}} = \frac{V_r (1-\eta)}{1-\mu} \tag{12}$$

Also, the variation of the V_r with respect to the thickness direction produces mechanical properties as a function of z. The volume fraction of nanofillers in the matrix can be expresses as:

$$V_r(z) = \left[\frac{\rho_r}{w_r \rho_M} - \frac{\rho_r}{\rho_M} + 1 \right]^{-1} \left(\frac{z}{h} + \frac{1}{2} \right)^{P} \tag{13}$$

in which ρ_r and ρ_M are mass densities of CNT and matrix, respectively. In addition, w_r is the mass fraction of nanofillers and can be calculated by:

$$w_r = \frac{M_r}{M_r + M_M} \tag{14}$$

where M_r and M_M are related to the mass of CNTs and matrix, respectively. It is worth mentioning that two versions of V_r can be defined in the problems of which agglomeration phenomenon is studied. The main difference between these two types is about the position of agglomerated nanoparticles and the matrix. In this case, the matrix is seemed to be in the bottom and the agglomerated CNTs are assumed to be at the top of the structure.

Now, the effective material properties can be reached following the relations of Eshelby-Mori-Tanaka micromechanical model [Shi, Feng, Huang et al. (2004)]. According to this model, the bulk moduli of inclusions can be written as:

$$K_{in}(z) = K_M + \frac{V_r \eta (\delta_r - 3K_M \alpha_r)}{3(\mu - V_r \eta + V_r \eta \alpha_r)} \tag{15}$$

where K_M is the bulk moduli of the matrix. Moreover, the shear moduli of inclusions can be introduced as:

$$G_{in}(z) = G_M + \frac{V_r \eta (\eta_r - 2G_M \beta_r)}{2(\mu - V_r \eta + V_r \eta \beta_r)} \tag{16}$$

where G_M is the shear moduli of matrix. Next, the bulk and shear moduli of the remnant parts can be formulated as:

$$K_{out}(z) = K_M + \frac{V_r(1-\eta)(\delta_r - 3K_M\alpha_r)}{3(1-\mu-V_r(1-\eta)+V_r(1-\eta)\alpha_r)} \tag{17}$$

$$G_{out}(z) = G_M + \frac{V_r(1-\eta)(\eta_r - 2G_M\beta_r)}{3(1-\mu-V_r(1-\eta)+V_r(1-\eta)\beta_r)} \tag{18}$$

In Eqs. (15)-(18), the mechanical terms α_r, β_r, δ_r and η_r can be calculated as:

$$\alpha_r = \frac{3(K_M + G_M) + k_r + l_r}{3(G_M + k_r)} \tag{19}$$

$$\beta_r = \frac{1}{5}\left(\frac{4G_M + 2k_r + l_r}{3(G_M + k_r)} + \frac{4G_M}{G_M + p_r} + \frac{2(G_M(3K_M + G_M) + G_M(3K_M + 7G_M))}{G_M(3K_M + G_M) + m_r(3K_M + 7G_M)}\right) \tag{20}$$

$$\delta_r = \frac{1}{3}\left(n_r + 2l_r + \frac{(2k_r + l_r)(3K_M + G_M - l_r)}{G_M + k_r}\right) \tag{21}$$

$$\eta_r = \frac{1}{5}\left(\frac{2}{3}(n_r - l_r) + \frac{8G_M p_r}{G_M + p_r} + \frac{(2k_r - l_r)(2G_M + l_r)}{3(G_M + k_r)} + \frac{8m_r G_M(3K_M + 4G_M)}{3K_M(m_r + G_M) + G_M(7m_r + G_M)}\right) \tag{22}$$

where k_r, l_r, m_r, n_r and p_r are the elastic Hill's coefficients of CNTs which can be different for each type of CNTs with respect to the chirality of the CNT. In this manuscript, the Hill's constants are employed for SWCNTs with chirality of (10,10) from the reference [Wang and Hu (2005)].

Based on the implemented homogenization scheme, the equivalent bulk moduli of the nanocomposite can be computed using the following formula:

$$K(z) = K_{out}\left(1 + \frac{\mu\left(\frac{K_{in}}{K_{out}} - 1\right)}{1 + (1-\mu)\left(\frac{K_{in}}{K_{out}} - 1\right)\frac{1+\nu_{out}}{3(1-\nu_{out})}}\right) \tag{23}$$

where ν_{out} is the Poisson's ratio of the matrix and can be defined as:

$$\nu_{out} = \frac{3K_{out} - 2G_{out}}{6K_{out} + 2G_{out}} \tag{24}$$

Also, the equivalent shear moduli can be computed as:

$$G(z) = G_{out}\left(1 + \frac{\mu\left(\frac{G_{in}}{G_{out}} - 1\right)}{1 + (1-\mu)\left(\frac{G_{in}}{G_{out}} - 1\right)\frac{8-10\nu_{out}}{15(1-\nu_{out})}}\right) \tag{25}$$

Finally, the equivalent Young moduli and Poisson's ratio of CNTR nanocomposites can be written in the following form:

$$E(z)=\frac{9K(z)\times G(z)}{3K(z)+G(z)} \tag{26}$$

$$\nu(z)=\frac{3K(z)-2G(z)}{6K(z)+2G(z)} \tag{27}$$

Moreover, the equivalent density of the CNTR nanocomposite can be formulated utilizing the fundamentals of mixture's rule as:

$$\rho(z)=(\rho_r-\rho_M)V_r+\rho_M \tag{28}$$

2.3 Refined parabolic plate theory

Present part is allocated to introduce a refined parabolic plate theory in order to derive the kinematic relations of the plate. In this theory, a shape function is employed to estimate the shear strain and stress. Here, the displacement field of plate can be written as:

$$\begin{aligned}
u_x(x,y,z,t)&=u(x,y,t)-z\frac{\partial w_b(x,y,t)}{\partial x}-f(z)\frac{\partial w_s(x,y,t)}{\partial x},\\
u_y(x,y,z,t)&=v(x,y,t)-z\frac{\partial w_b(x,y,t)}{\partial y}-f(z)\frac{\partial w_s(x,y,t)}{\partial y},\\
u_z(x,y,z,t)&=w_b(x,y,t)+w_s(x,y,t)
\end{aligned} \tag{29}$$

In above equations, u and v are longitudinal and transverse displacements of the mid-surface, respectively; also, w_b and w_s are the bending and shear deflections through z-axis, respectively. In addition, $f(z)$ stands for the shape function of the theorem. In this paper this function is considered to be $f(z)=-\frac{z}{4}+\frac{5z^3}{3h^2}$. Now, the nonzero strains of the plate can be expressed by following equations:

$$\begin{Bmatrix}\varepsilon_{xx}\\ \varepsilon_{yy}\\ \gamma_{xy}\end{Bmatrix}=\begin{Bmatrix}\varepsilon^0_{xx}\\ \varepsilon^0_{yy}\\ \gamma^0_{xy}\end{Bmatrix}+z\begin{Bmatrix}\kappa^b_{xx}\\ \kappa^b_{yy}\\ \kappa^b_{xy}\end{Bmatrix}+f(z)\begin{Bmatrix}\kappa^s_{xx}\\ \kappa^s_{yy}\\ \kappa^s_{xy}\end{Bmatrix},\qquad \begin{Bmatrix}\gamma_{xz}\\ \gamma_{yz}\end{Bmatrix}=\begin{Bmatrix}\gamma^0_{xz}\\ \gamma^0_{yz}\end{Bmatrix} \tag{30}$$

where

$$\begin{Bmatrix} \varepsilon_{xx}^0 \\ \varepsilon_{yy}^0 \\ \gamma_{xy}^0 \end{Bmatrix} = \begin{Bmatrix} \dfrac{\partial u}{\partial x} \\ \dfrac{\partial v}{\partial y} \\ \dfrac{\partial u}{\partial y} + \dfrac{\partial v}{\partial x} \end{Bmatrix}, \quad \begin{Bmatrix} \kappa_{xx}^b \\ \kappa_{yy}^b \\ \kappa_{xy}^b \end{Bmatrix} = \begin{Bmatrix} -\dfrac{\partial^2 w_b}{\partial x^2} \\ -\dfrac{\partial^2 w_b}{\partial y^2} \\ -2\dfrac{\partial^2 w_b}{\partial x \partial y} \end{Bmatrix}, \quad \begin{Bmatrix} \kappa_{xx}^s \\ \kappa_{yy}^s \\ \kappa_{xy}^s \end{Bmatrix} = \begin{Bmatrix} -\dfrac{\partial^2 w_s}{\partial x^2} \\ -\dfrac{\partial^2 w_s}{\partial y^2} \\ -2\dfrac{\partial^2 w_s}{\partial x \partial y} \end{Bmatrix}, \quad \begin{Bmatrix} \gamma_{xz}^0 \\ \gamma_{yz}^0 \end{Bmatrix} = \begin{Bmatrix} \dfrac{\partial w_s}{\partial x} \\ \dfrac{\partial w_s}{\partial y} \end{Bmatrix} \tag{31}$$

2.4 Derivation of motion equations

In this section, the equations of motion are going to be developed in the framework of a Hamiltonian approach. Actually, Hamilton's principle can be defined as:

$$\int_0^t \delta(U+V)dt = 0 \tag{32}$$

where U and V account for strain energy and work done by external forces, respectively. The variation of strain energy is written as:

$$\begin{aligned} \delta U &= \int_V \left(\sigma_{xx}\delta\varepsilon_{xx} + \sigma_{yy}\delta\varepsilon_{yy} + \sigma_{xy}\delta\gamma_{xy} + \sigma_{xz}\delta\gamma_{xz} + \sigma_{yz}\delta\gamma_{yz} \right) dV \\ &= \int_0^b \int_0^a \begin{pmatrix} N_{xx}\delta\varepsilon_{xx}^0 + M_{xx}^b \delta\kappa_{xx}^b + M_{xx}^s \delta\kappa_{xx}^s + N_{yy}\delta\varepsilon_{yy}^0 + \\ M_{yy}^b \delta\kappa_{yy}^b + M_{yy}^s \delta\kappa_{yy}^s + N_{xy}\delta\gamma_{xy}^0 + M_{xy}^b \delta\kappa_{xy}^b + \\ M_{xy}^s \delta\kappa_{xy}^s + Q_{xz}\delta\gamma_{xz}^0 + Q_{yz}\delta\gamma_{yz}^0 \end{pmatrix} dxdy \end{aligned} \tag{33}$$

in above equation, the axial forces and bending moments can be defined as:

$$\begin{aligned} &\left(N_{ij}, M_{ij}^b, M_{ij}^s \right) = \int_{-h/2}^{h/2} \left(1, z, f(z)\right) \sigma_{ij} dz, \quad \left(i, j = x, y\right), \\ &Q_k = \int_{-h/2}^{h/2} g(z)\sigma_k dz, \quad \left(k = xz, yz\right) \end{aligned} \tag{34}$$

where $g(z) = 1 - \frac{df}{dz}$. The variation of work done by buckling load can be expressed as:

$$\delta V = \int_0^b \int_0^a -N^b \left(\frac{\partial(w_b + w_s)}{\partial x} \frac{\partial \delta(w_b + w_s)}{\partial x} + \frac{\partial(w_b + w_s)}{\partial y} \frac{\partial \delta(w_b + w_s)}{\partial y} \right) dxdy \tag{35}$$

By substituting Eqs. (33) and (35) into Eq. (32) and setting the coefficients of δu, δv, δw_b and δw_s to zero, the Euler-Lagrange equations of multi-scale hybrid nanocomposite plates can be written as:

$$\frac{\partial N_{xx}}{\partial x} + \frac{\partial N_{xy}}{\partial y} = 0 \tag{36}$$

$$\frac{\partial N_{xy}}{\partial x}+\frac{\partial N_{yy}}{\partial y}=0 \tag{37}$$

$$\frac{\partial^2 M^b_{xx}}{\partial x^2}+2\frac{\partial^2 M^b_{xy}}{\partial x\partial y}+\frac{\partial^2 M^b_{yy}}{\partial y^2}-N^b\nabla^2\left(w_b+w_s\right)=0 \tag{38}$$

$$\frac{\partial^2 M^s_{xx}}{\partial x^2}+2\frac{\partial^2 M^s_{xy}}{\partial x\partial y}+\frac{\partial^2 M^s_{yy}}{\partial y^2}+\frac{\partial Q_{xz}}{\partial x}+\frac{\partial Q_{yz}}{\partial y}-N^b\nabla^2\left(w_b+w_s\right)=0 \tag{39}$$

where ∇^2 stands for the Laplacian operator.

2.5 Constitutive equations

Herein, the elastic stress-strain relations of orthotropic composite materials are reviewed for the purpose of deriving the fundamental elastic equations of such solids. Here, following constitutive equations can be expressed as:

$$\sigma_{ij}=C_{ijkl}\varepsilon_{kl} \tag{40}$$

where σ_{ij}, ε_{kl} and C_{ijkl} represent the components of second-order stress tensor, second-order strain tensor and fourth-order elastic tensor, respectively. Therefore, these relations can be modified as follows for plates:

$$\begin{bmatrix}\sigma_{xx}\\ \sigma_{yy}\\ \sigma_{yz}\\ \sigma_{xz}\\ \sigma_{xy}\end{bmatrix}=\begin{bmatrix}Q_{11} & Q_{12} & 0 & 0 & 0\\ Q_{12} & Q_{22} & 0 & 0 & 0\\ 0 & 0 & Q_{44} & 0 & 0\\ 0 & 0 & 0 & Q_{55} & 0\\ 0 & 0 & 0 & 0 & Q_{66}\end{bmatrix}\begin{bmatrix}\varepsilon_{xx}\\ \varepsilon_{yy}\\ \varepsilon_{yz}\\ \varepsilon_{xz}\\ \varepsilon_{xy}\end{bmatrix} \tag{41}$$

where

$$Q_{11}=\frac{E_{11}}{1-\nu_{12}\nu_{21}},\quad Q_{12}=\frac{\nu_{12}E_{22}}{1-\nu_{12}\nu_{21}},\quad Q_{22}=\frac{E_{22}}{1-\nu_{12}\nu_{21}},$$
$$Q_{44}=G_{23},\quad Q_{55}=G_{13},\quad Q_{66}=G_{12} \tag{42}$$

Now, integrating from Eq. (41) with respect to thickness direction, *z*- axis, the following resultant forces and moments can be achieved:

$$\begin{bmatrix} N_{xx} \\ N_{yy} \\ N_{xy} \\ M^b_{xx} \\ M^b_{yy} \\ M^b_{xy} \\ M^s_{xx} \\ M^s_{yy} \\ M^s_{xy} \end{bmatrix} = \begin{bmatrix} A_{11} & A_{12} & 0 & B_{11} & B_{12} & 0 & B^s_{11} & B^s_{12} & 0 \\ A_{12} & A_{22} & 0 & B_{12} & B_{22} & 0 & B^s_{12} & B^s_{22} & 0 \\ 0 & 0 & A_{66} & 0 & 0 & B_{66} & 0 & 0 & B^s_{66} \\ B_{11} & B_{12} & 0 & D_{11} & D_{12} & 0 & D^s_{11} & D^s_{12} & 0 \\ B_{12} & B_{22} & 0 & D_{12} & D_{22} & 0 & D^s_{12} & D^s_{22} & 0 \\ 0 & 0 & B_{66} & 0 & 0 & D_{66} & 0 & 0 & D^s_{66} \\ B^s_{11} & B^s_{12} & 0 & D^s_{11} & D^s_{12} & 0 & H^s_{11} & H^s_{12} & 0 \\ B^s_{12} & B^s_{22} & 0 & D^s_{12} & D^s_{22} & 0 & H^s_{12} & H^s_{22} & 0 \\ 0 & 0 & B^s_{66} & 0 & 0 & D^s_{66} & 0 & 0 & H^s_{66} \end{bmatrix} \begin{bmatrix} \frac{\partial u}{\partial x} \\ \frac{\partial v}{\partial y} \\ \frac{\partial u}{\partial y} + \frac{\partial v}{\partial x} \\ -\frac{\partial^2 w_b}{\partial x^2} \\ -\frac{\partial^2 w_b}{\partial y^2} \\ -2\frac{\partial^2 w_b}{\partial x \partial y} \\ -\frac{\partial^2 w_s}{\partial x^2} \\ -\frac{\partial^2 w_s}{\partial y^2} \\ -2\frac{\partial^2 w_s}{\partial x \partial y} \end{bmatrix}, \quad \begin{bmatrix} Q_{xz} \\ Q_{yz} \end{bmatrix} = \begin{bmatrix} A^s_{44} & 0 \\ 0 & A^s_{55} \end{bmatrix} \begin{bmatrix} \frac{\partial w_s}{\partial x} \\ \frac{\partial w_s}{\partial y} \end{bmatrix} \tag{43}$$

where

$$\left[A_n, B_n, B^s_n, D_n, D^s_n, H^s_n\right] = \int_{-h/2}^{h/2} \left[1, z, f(z), z^2, zf(z), f^2(z)\right] Q_n(z) dz, \quad n = (11,12,22,66)$$
$$\left[A^s_{44}, A^s_{55}\right] = \int_{-h/2}^{h/2} \left[Q_{44}(z), Q_{55}(z)\right] g^2(z) dz \tag{44}$$

2.6 Governing equations

In this section, inserting Eq. (43) in Eqs. (36)-(39), the governing equations of multi-scale hybrid nanocomposite plates can be expressed in the following form:

$$A_{11}\frac{\partial^2 u}{\partial x^2} + A_{66}\frac{\partial^2 u}{\partial y^2} + \left(A_{12} + A_{66}\right)\frac{\partial^2 v}{\partial x \partial y} - B_{11}\frac{\partial^3 w_b}{\partial x^3} - \left(B_{12} + 2B_{66}\right)\frac{\partial^3 w_b}{\partial x \partial y^2}$$
$$-B^s_{11}\frac{\partial^3 w_s}{\partial x^3} - \left(B^s_{12} + 2B^s_{66}\right)\frac{\partial^3 w_s}{\partial x \partial y^2} = 0 \tag{45}$$

$$\left(A_{12} + A_{66}\right)\frac{\partial^2 u}{\partial x \partial y} + A_{66}\frac{\partial^2 v}{\partial x^2} + A_{22}\frac{\partial^2 v}{\partial y^2} - \left(B_{12} + 2B_{66}\right)\frac{\partial^3 w_b}{\partial x^2 \partial y} - B_{22}\frac{\partial^3 w_b}{\partial y^3}$$
$$-\left(B^s_{12} + 2B^s_{66}\right)\frac{\partial^3 w_s}{\partial x^2 \partial y} - B^s_{22}\frac{\partial^3 w_s}{\partial y^3} = 0 \tag{46}$$

$$B_{11}\frac{\partial^3 u}{\partial x^3} + \left(B_{12} + 2B_{66}\right)\left(\frac{\partial^3 u}{\partial x \partial y^2} + \frac{\partial^3 v}{\partial x^2 \partial y}\right) + B_{22}\frac{\partial^3 v}{\partial y^3} - D_{11}\frac{\partial^4 w_b}{\partial x^4} - 2\left(D_{12} + 2D_{66}\right)\frac{\partial^4 w_b}{\partial x^2 \partial y^2}$$
$$-D_{22}\frac{\partial^4 w_b}{\partial y^4} - D^s_{11}\frac{\partial^4 w_s}{\partial x^4} - 2\left(D^s_{12} + 2D^s_{66}\right)\frac{\partial^4 w_s}{\partial x^2 \partial y^2} - D^s_{22}\frac{\partial^4 w_s}{\partial y^4} - N^b\left(\frac{\partial^2 w}{\partial x^2} + \frac{\partial^2 w}{\partial y^2}\right) = 0 \tag{47}$$

$$\begin{aligned}
&B_{11}^s \frac{\partial^3 u}{\partial x^3} + \left(B_{12}^s + 2B_{66}^s\right)\left(\frac{\partial^3 u}{\partial x \partial y^2} + \frac{\partial^3 v}{\partial x^2 \partial y}\right) + B_{22}^s \frac{\partial^3 v}{\partial y^3} - D_{11}^s \frac{\partial^4 w_b}{\partial x^4} - 2\left(D_{12}^s + 2D_{66}^s\right)\frac{\partial^4 w_b}{\partial x^2 \partial y^2} \\
&-D_{22}^s \frac{\partial^4 w_b}{\partial y^4} - H_{11}^s \frac{\partial^4 w_s}{\partial x^4} - 2\left(H_{12}^s + 2H_{66}^s\right)\frac{\partial^4 w_s}{\partial x^2 \partial y^2} - H_{22}^s \frac{\partial^4 w_s}{\partial y^4} - N^b\left(\frac{\partial^2 w}{\partial x^2} + \frac{\partial^2 w}{\partial y^2}\right) + \\
&A_{55}^s \frac{\partial^2 w_s}{\partial x^2} + A_{44}^s \frac{\partial^2 w_s}{\partial y^2} = 0
\end{aligned} \tag{48}$$

3 Analytical solution

Up to now, many analytical and numerical methods are found to be utilized for the goal of solving the buckling problem of plates. Herein, the governing equations achieved in Eqs. (41)-(44) will be solved in the framework of Galerkin's method which is one of the best analytical solutions for static and dynamic problems. In this method the displacement field of a plate can be defined as:

$$\begin{aligned}
u &= \sum_{m=1}^{\infty}\sum_{n=1}^{\infty} U_{mn} \frac{\partial X_m(x)}{\partial x} Y_n(y), \\
v &= \sum_{m=1}^{\infty}\sum_{n=1}^{\infty} V_{mn} X_m(x) \frac{\partial Y_n(y)}{\partial y}, \\
w_b &= \sum_{m=1}^{\infty}\sum_{n=1}^{\infty} W_{bmn} X_m(x) Y_n(y), \\
w_s &= \sum_{m=1}^{\infty}\sum_{n=1}^{\infty} W_{smn} X_m(x) Y_n(y)
\end{aligned} \tag{49}$$

where U_{mn}, V_{mn}, W_{bmn} and W_{smn} are unknown coefficients. Moreover, X_m and Y_n are trigonometric functions in terms of x and y, respectively; these functions are majorly presented to satisfy the BCs on edges of the plate. It is worth mentioning that in the present paper effects of various BCs are included. Here, by inserting Eq. (49) in Eqs. (45)-(48) and integrating over the cross-section area of the plate results in the following eigenvalue problem:

$$\left[K\right]_{4\times 4}\begin{bmatrix} U_{mn} \\ V_{mn} \\ W_{bmn} \\ W_{smn} \end{bmatrix} = 0 \tag{50}$$

where K is stiffness matrix. The corresponding arrays of stiffness matrix can be calculated a

$$k_{11} = A_{11}\int_0^b\int_0^a \frac{\partial X_m(x)}{\partial x} Y_n(y) \frac{\partial^3 X_m(x)}{\partial x^3} Y_n(y) dxdy + A_{66}\int_0^b\int_0^a \frac{\partial X_m(x)}{\partial x} Y_n(y) \frac{\partial X_m(x)}{\partial x} \frac{\partial^2 Y_n(y)}{\partial y^2} dxdy \tag{51}$$

$$k_{12} = \left(A_{12} + A_{66}\right)\int_0^b\int_0^a \frac{\partial X_m(x)}{\partial x} Y_n(y) \frac{\partial X_m(x)}{\partial x} \frac{\partial^2 Y_n(y)}{\partial y^2} dxdy \tag{52}$$

$$k_{13} = -B_{11}\int_0^b\int_0^a \frac{\partial X_m(x)}{\partial x} Y_n(y) \frac{\partial^3 X_m(x)}{\partial x^3} Y_n(y) dxdy - \left(B_{12} + 2B_{66}\right)\int_0^b\int_0^a \frac{\partial X_m(x)}{\partial x} Y_n(y) \frac{\partial X_m(x)}{\partial x} \frac{\partial^2 Y_n(y)}{\partial y^2} dxdy \quad (53)$$

$$k_{14} = -B_{11}^s\int_0^b\int_0^a \frac{\partial X_m(x)}{\partial x} Y_n(y) \frac{\partial^3 X_m(x)}{\partial x^3} Y_n(y) dxdy - \left(B_{12}^s + 2B_{66}^s\right)\int_0^b\int_0^a \frac{\partial X_m(x)}{\partial x} Y_n(y) \frac{\partial X_m(x)}{\partial x} \frac{\partial^2 Y_n(y)}{\partial y^2} dxdy \quad (54)$$

$$k_{21} = \left(A_{12} + A_{66}\right)\int_0^b\int_0^a X_m(x) \frac{\partial Y_n(y)}{\partial y} \frac{\partial^2 X_m(x)}{\partial x^2} \frac{\partial Y_n(y)}{\partial y} dxdy \quad (55)$$

$$k_{22} = A_{66}\int_0^b\int_0^a X_m(x) \frac{\partial Y_n(y)}{\partial y} \frac{\partial^2 X_m(x)}{\partial x^2} \frac{\partial Y_n(y)}{\partial y} dxdy + A_{22}\int_0^b\int_0^a X_m(x) \frac{\partial Y_n(y)}{\partial y} X_m(x) \frac{\partial^3 Y_n(y)}{\partial y^3} dxdy \quad (56)$$

$$k_{23} = -\left(B_{12} + 2B_{66}\right)\int_0^b\int_0^a X_m(x) \frac{\partial Y_n(y)}{\partial y} \frac{\partial^2 X_m(x)}{\partial x^2} \frac{\partial Y_n(y)}{\partial y} dxdy - B_{22}\int_0^b\int_0^a X_m(x) \frac{\partial Y_n(y)}{\partial y} X_m(x) \frac{\partial^3 Y_n(y)}{\partial y^3} dxdy \quad (57)$$

$$k_{24} = -\left(B_{12}^s + 2B_{66}^s\right)\int_0^b\int_0^a X_m(x) \frac{\partial Y_n(y)}{\partial y} \frac{\partial^2 X_m(x)}{\partial x^2} \frac{\partial Y_n(y)}{\partial y} dxdy - B_{22}^s\int_0^b\int_0^a X_m(x) \frac{\partial Y_n(y)}{\partial y} X_m(x) \frac{\partial^3 Y_n(y)}{\partial y^3} dxdy \quad (58)$$

$$k_{31} = B_{11}\int_0^b\int_0^a X_m(x) Y_n(y) \frac{\partial^4 X_m(x)}{\partial x^4} Y_n(y) dxdy + \left(B_{12} + 2B_{66}\right)\int_0^b\int_0^a X_m(x) Y_n(y) \frac{\partial^2 X_m(x)}{\partial x^2} \frac{\partial^2 Y_n(y)}{\partial y^2} dxdy \quad (59)$$

$$k_{32} = \left(B_{12} + 2B_{66}\right)\int_0^b\int_0^a X_m(x) Y_n(y) \frac{\partial^2 X_m(x)}{\partial x^2} \frac{\partial^2 Y_n(y)}{\partial y^2} dxdy + B_{22}\int_0^b\int_0^a X_m(x) Y_n(y) X_m(x) \frac{\partial^4 Y_n(y)}{\partial y^4} dxdy \quad (60)$$

$$\begin{aligned} k_{33} = {} & -D_{11}\int_0^b\int_0^a X_m(x) Y_n(y) \frac{\partial^4 X_m(x)}{\partial x^4} Y_n(y) dxdy - 2\left(D_{12} + 2D_{66}\right)\int_0^b\int_0^a X_m(x) Y_n(y) \frac{\partial^2 X_m(x)}{\partial x^2} \frac{\partial^2 Y_n(y)}{\partial y^2} dxdy \\ & - D_{22}\int_0^b\int_0^a X_m(x) Y_n(y) X_m(x) \frac{\partial^4 Y_n(y)}{\partial y^4} dxdy - \\ & N^b\left(\int_0^b\int_0^a \frac{\partial^2 X_m(x)}{\partial x^2} Y_n(y) X_m(x) Y_n(y) dxdy + \int_0^b\int_0^a X_m(x) Y_n(y) X_m(x) \frac{\partial^2 Y_n(y)}{\partial y^2} dxdy\right) \end{aligned} \quad (61)$$

$$\begin{aligned} k_{34} = {} & -D_{11}^s\int_0^b\int_0^a X_m(x) Y_n(y) \frac{\partial^4 X_m(x)}{\partial x^4} Y_n(y) dxdy - 2\left(D_{12}^s + 2D_{66}^s\right)\int_0^b\int_0^a X_m(x) Y_n(y) \frac{\partial^2 X_m(x)}{\partial x^2} \frac{\partial^2 Y_n(y)}{\partial y^2} dxdy \\ & - D_{22}^s\int_0^b\int_0^a X_m(x) Y_n(y) X_m(x) \frac{\partial^4 Y_n(y)}{\partial y^4} dxdy - \\ & N^b\left(\int_0^b\int_0^a \frac{\partial^2 X_m(x)}{\partial x^2} Y_n(y) X_m(x) Y_n(y) dxdy + \int_0^b\int_0^a X_m(x) Y_n(y) X_m(x) \frac{\partial^2 Y_n(y)}{\partial y^2} dxdy\right) \end{aligned} \quad (62)$$

$$k_{41} = B_{11}^s\int_0^b\int_0^a X_m(x) Y_n(y) \frac{\partial^4 X_m(x)}{\partial x^4} Y_n(y) dxdy + \left(B_{12}^s + 2B_{66}^s\right)\int_0^b\int_0^a \frac{\partial^2 X_m(x)}{\partial x^2} Y_n(y) X_m(x) \frac{\partial^2 Y_n(y)}{\partial y^2} dxdy \quad (63)$$

$$k_{42}=\left(B_{12}^{s}+2B_{66}^{s}\right)\int_{0}^{b}\int_{0}^{a}X_m(x)Y_n(y)\frac{\partial^2 X_m(x)}{\partial x^2}\frac{\partial^2 Y_n(y)}{\partial y^2}dxdy+B_{22}^{s}\int_{0}^{b}\int_{0}^{a}X_m(x)Y_n(y)X_m(x)\frac{\partial^4 Y_n(y)}{\partial y^4}dxdy \tag{64}$$

$$\begin{aligned}k_{43}=&-D_{11}^{s}\int_{0}^{b}\int_{0}^{a}X_m(x)Y_n(y)\frac{\partial^4 X_m(x)}{\partial x^4}Y_n(y)dxdy-2\left(D_{12}^{s}+2D_{66}^{s}\right)\int_{0}^{b}\int_{0}^{a}X_m(x)Y_n(y)\frac{\partial^2 X_m(x)}{\partial x^2}\frac{\partial^2 Y_n(y)}{\partial y^2}dxdy\\&-D_{22}^{s}\int_{0}^{b}\int_{0}^{a}X_m(x)Y_n(y)X_m(x)\frac{\partial^4 Y_n(y)}{\partial y^4}dxdy-\\&N^{b}\left(\int_{0}^{b}\int_{0}^{a}\frac{\partial^2 X_m(x)}{\partial x^2}Y_n(y)X_m(x)Y_n(y)dxdy+\int_{0}^{b}\int_{0}^{a}X_m(x)Y_n(y)X_m(x)\frac{\partial^2 Y_n(y)}{\partial y^2}dxdy\right)\end{aligned} \tag{65}$$

$$\begin{aligned}k_{44}=&-H_{11}^{s}\int_{0}^{b}\int_{0}^{a}X_m(x)Y_n(y)\frac{\partial^4 X_m(x)}{\partial x^4}Y_n(y)dxdy-2\left(H_{12}^{s}+2H_{66}^{s}\right)\int_{0}^{b}\int_{0}^{a}X_m(x)Y_n(y)\frac{\partial^2 X_m(x)}{\partial x^2}\frac{\partial^2 Y_n(y)}{\partial y^2}dxdy\\&-H_{22}^{s}\int_{0}^{b}\int_{0}^{a}X_m(x)Y_n(y)X_m(x)\frac{\partial^4 Y_n(y)}{\partial y^4}dxdy+A_{44}^{s}\int_{0}^{b}\int_{0}^{a}X_m(x)Y_n(y)\frac{\partial^2 X_m(x)}{\partial x^2}Y_n(y)dxdy-\\&N^{b}\left(\int_{0}^{b}\int_{0}^{a}\frac{\partial^2 X_m(x)}{\partial x^2}Y_n(y)X_m(x)Y_n(y)dxdy+\int_{0}^{b}\int_{0}^{a}X_m(x)Y_n(y)X_m(x)\frac{\partial^2 Y_n(y)}{\partial y^2}dxdy\right)+\\&A_{44}^{s}\int_{0}^{b}\int_{0}^{a}X_m(x)Y_n(y)X_m(x)\frac{\partial^2 Y_n(y)}{\partial y^2}dxdy\end{aligned} \tag{66}$$

In order to solve this eigenvalue problem, the determinant of coefficient matrix in the left hand side of Eq. (50) shall be set to zero:

$$\left|\left[K\right]_{4\times 4}\right|=0 \tag{67}$$

Once Eq. (67) is solved for N^b, the critical buckling load of multi-scale hybrid nanocomposite plate can be obtained.

4 Numerical results and discussion

In this section, a series of illustrations are presented in order to clarify the effect of various parameters on the critical stability load behaviors of multi-scale hybrid nanocomposite structures. Basically, the plate is supposed to be made of epoxy and it is reinforced with CF and CNT. Material properties of CFs are achieved from Ebrahimi et al. [Ebrahimi and Habibi (2018)]. The mechanical properties of SWCNT (10,10) which are used here can be found in the reference [Wang and Hu (2005)]. Moreover, the material properties of the matrix are as same as those implemented in the reference [Fantuzzi et al. (2017)]. The presented results are validated by comparing the vibrational results of this model with those of former researches. The results of this comparison are tabulated in Tab. 1 which indicates on the efficiency of the presented model.

Table 1: Comparison of the dimensionless fundamental frequency of SSSS GPLs reinforced nanocomposite square plates for various distribution patterns of nanofillers

Distribution type	[García-Macías, Rodriguez-Tembleque and Sáez (2018)]	[Song, Kitipornchai and Yang (2017)]	Present
Pure epoxy	0.058	0.058	0.057
UD	0.121	0.122	0.118
FG-O	0.097	0.102	0.100
FG-X	0.141	0.138	0.128
FG-A	0.117	0.112	0.118

In this research, plate's thickness is supposed to be h=5 cm. In this section, effects of different edge conditions are covered. Furthermore, efficiency of the presented model is examined and the results, tabulated in Tab. 1, show that this model can accurately predict the mechanical responses of composite plates reinforced with CNTs. Here, the dimensionless form of buckling load can be presented as:

$$\Omega = \frac{3N^b a^2 \left(1-\nu_M{}^2\right)}{25E_M h^3} \tag{68}$$

Fig. 2 is plotted to show the influence of different aspect ratios on the critical buckling load of multi-scale hybrid nanocomposite plates while the volume fraction of clusters is assumed to be changed. In this case, all of the CNTs are considered to be inside the clusters, means $\mu<\eta$, η=1. According to the figure, buckling load diminishes continuously as aspect ratio becomes greater. Moreover, the greater is the clusters' volume fraction, the higher is the dimensionless buckling load. Therefore, clusters' density can amplify the dimensionless buckling load with its increase. On the other hand, effect of BCs is included briefly. Indeed, two common types of edge conditions, namely SSSS and CCCC, are covered and it can be seen that whenever a fully clamped structure is implemented, the mechanical response can be higher than the situation of which simply supported plates are used. Once taking a precise look at the figure, one can realize that changes in the amount of clusters' volume fraction can be more sensed in SSSS plates in comparison with the CCCC ones.

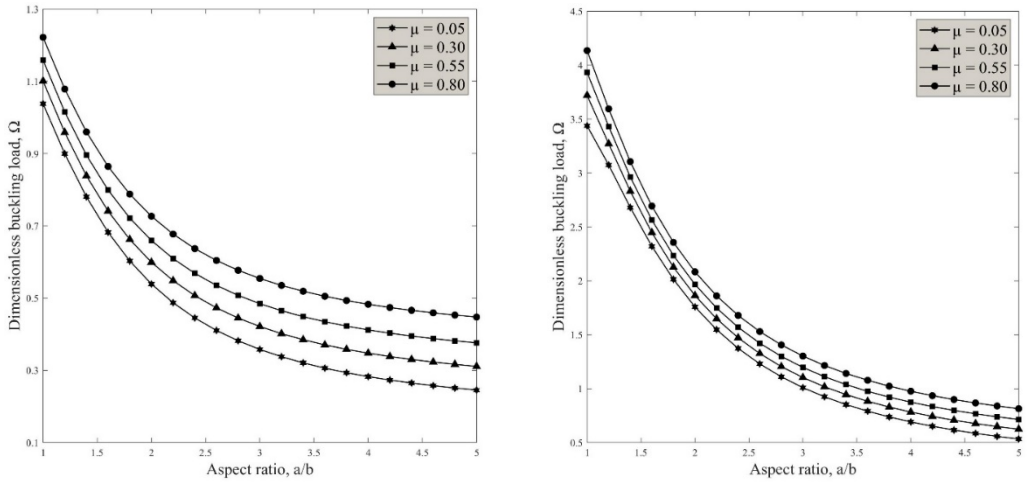

(a) SSSS **(b) CCCC**

Figure 2: Variation of first dimensionless buckling load of agglomerated multi-scale hybrid nanocomposite square plates versus aspect ratio for various values of μ by considering the boundary conditions effect (b/h=30, P=1, w_r=0.1, η=1, V_F=0.2)

Furthermore, coupled effects of gradient index, clusters' volume fraction and volume fraction of CNTs inside the cluster are included in Fig. 3. It is clear that gradient index has enough potential to lessen the dimensionless buckling load with its increase. So, it may be a better choice to use small values of gradient index to enlarge the buckling load of the plate. In addition, the influence of volume fraction of clusters inside a nanocomposite can be observed here as well as before. In fact, higher clusters' volume fraction amounts correspond with greater dimensionless buckling loads. Moreover, smaller amounts are assigned to the critical buckling load whenever higher values are considered for the volume fraction of CNTs inside the cluster. In other words, in practical applications, the stability limit of nanocomposites with fully agglomerated CNTs is very smaller than those with partially agglomerated CNTs. Thus, it can be concluded that clusters' volume fraction and the volume fraction of CNTs inside the cluster possess two completely different influences on the buckling behaviors of multi-scale hybrid nanocomposite plates.

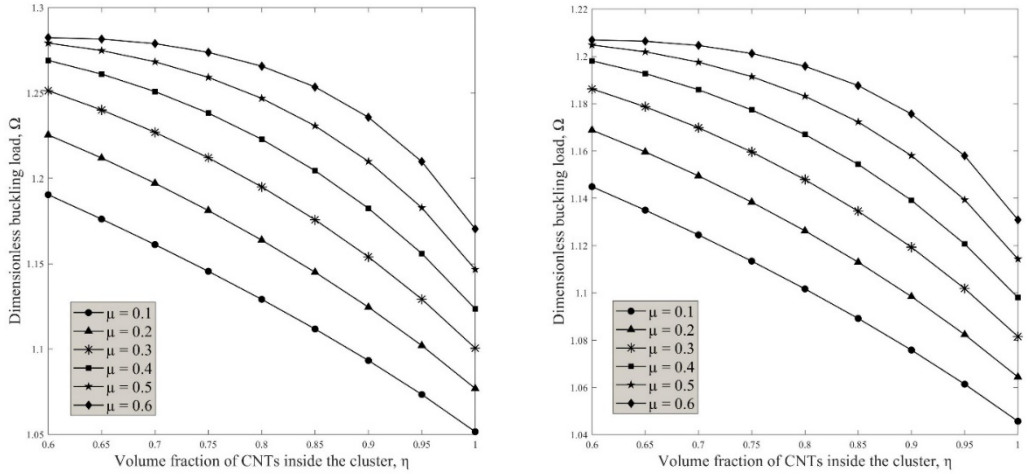

(a) *P*=1 **(b) *P*=2**

Figure 3: Variation of dimensionless buckling load of SSSS square multi-scale nanocomposite plates versus volume fraction of CNTs inside the cluster (η) for various volume fractions of clusters (μ) for (a) P=1, and (b) P=2 (a/h=30, w_r=0.1, V_F=0.2)

Fig. 4 is majorly presented to survey the effect of mass fraction of CNTs instead of clusters' volume fraction on the dimensionless buckling load of SSSS square plates made of multi-scale hybrid nanocomposites. Based on this diagram, it can be understood that utilizing higher mass fractions for nanoparticles reveals greater stability responses. This phenomenon can be authenticated taking a brief look on the definition of the w_r. In fact, mass fraction of CNTs in the matrix depends on the equivalent mass of CNTs inside the matrix. Thus, greater values for this fraction corresponds with a stiffer continuum. In other words, whenever w_r is increased, the effective stiffness of the system is added. According to this issue, it is believable to reach higher dimensionless buckling loads in the cases which great mass fractions are utilized for the nanofillers. Besides, the decreasing influences of gradient index and volume fraction of CNTs inside the cluster can be observed again in this diagram.

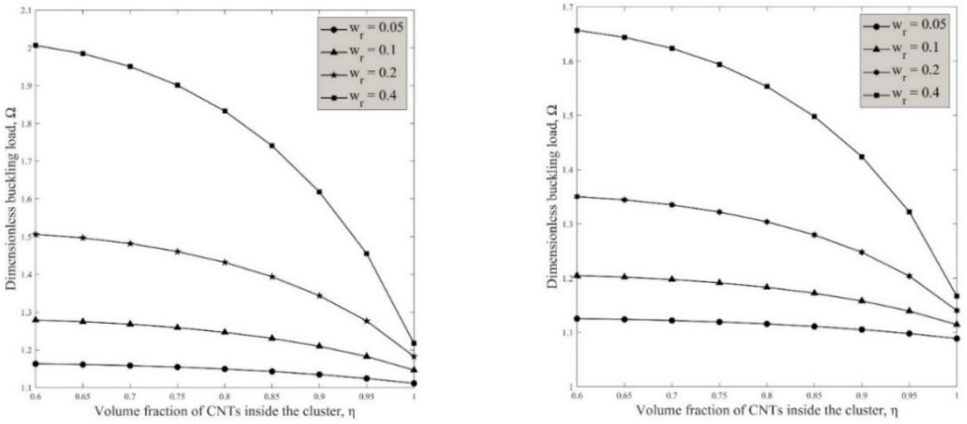

(a) *P*=1 **(b) *P*=2**

Figure 4: Variation of dimensionless buckling load of SSSS square multi-scale nanocomposite plates versus volume fraction of CNTs inside the cluster (η) for various mass fractions of the CNTs (w_r) for (a) P=1, and (b) P=2 (a/h=30, μ=0.5, V_F=0.2)

Thereafter, the effect of adding CFs' volume fraction on the variation of critical buckling load versus volume fraction of clusters is highlighted in the framework of Fig. 5. Also, CNTs' mass fraction has been changed to see its effect on the dimensionless buckling load. Obviously, it can be perceived that the buckling response can be aggrandized once either μ or w_r is added. In addition to this increasing effect, another stiffness-hardening trend can be observed which is dedicated to the volume fraction of CFs. In other words, the system can be prepared to tolerate greater buckling loads by considering a bigger value for the CFs' volume fraction.

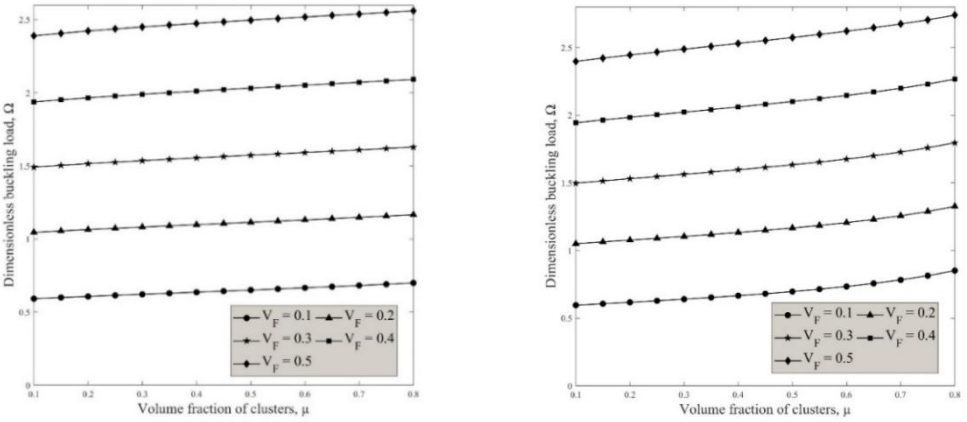

(a) w_r=0.1 (b) w_r=0.4

Figure 5: Variation of dimensionless buckling load of SSSS square multi-scale nanocomposite plates versus volume fractions of clusters (μ) for various volume fractions of carbon fibers (V_F) for (a) w_r=0.1, and (b) w_r=0.4 (a/h=30, P=2, η=1)

The combined effects of aspect ratio, BCs and agglomeration type are surveyed in Fig. 6 by plotting the variation of dimensionless buckling load versus clusters' volume fraction. It is clear that the plate can be subjected to higher buckling loads whenever volume fraction of clusters is increased. Moreover, choosing a higher aspect ratio results in a decrease in the amount of mechanical response. Actually, once higher aspect ratios are selected, the structure becomes narrow and it can endure lower loads. It is worth mentioning that effect of changing aspect ratio from 1 to 2 is more than the situation that it is changed from 2 to 3. As a logical phenomenon, it is shown that fully clamped plates are stiffer than simply supported ones; henceforward, they are able to endure higher buckling loads. As the most crucial highlight of this figure, one should pay attention that in the case of full agglomeration the dimensionless buckling load reaches its minimum magnitude. Indeed, in the case of CNTs' partial agglomeration ($\mu<\eta$, $\eta\neq1$), greater buckling loads can be supported by the nanocomposite.

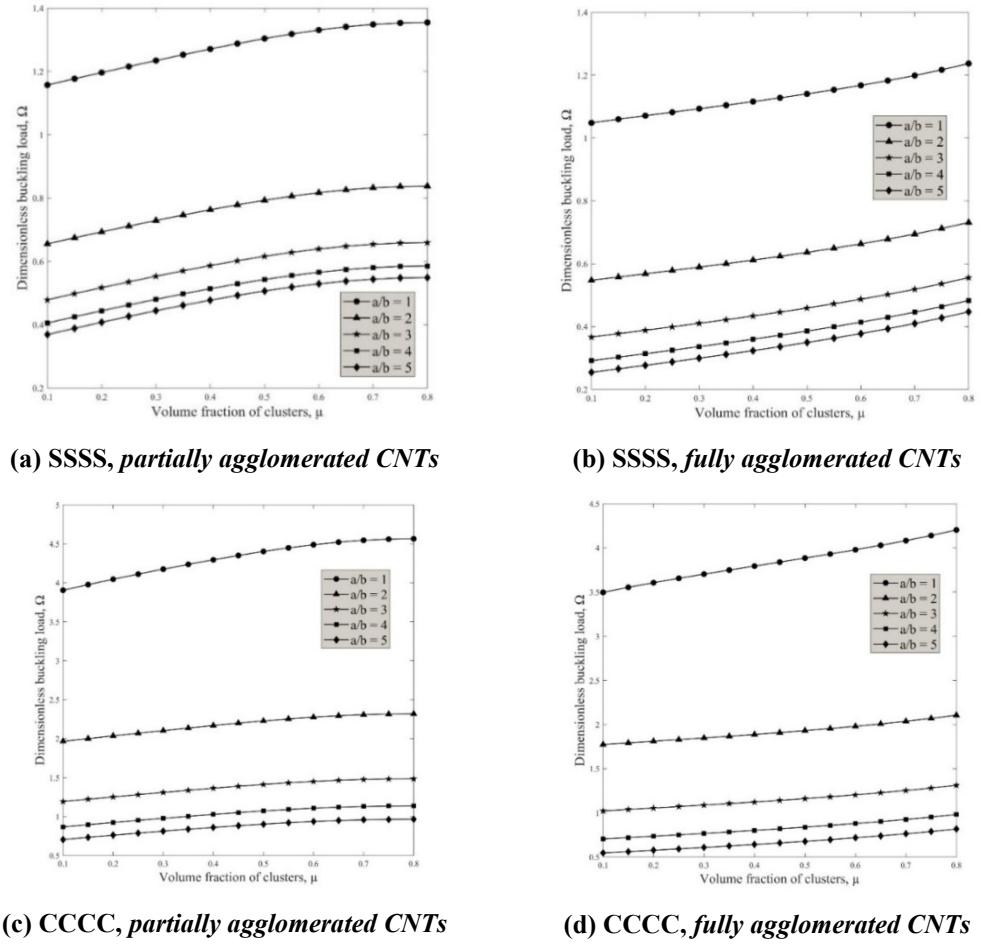

(a) SSSS, *partially agglomerated CNTs* **(b) SSSS, *fully agglomerated CNTs***

(c) CCCC, *partially agglomerated CNTs* **(d) CCCC, *fully agglomerated CNTs***

Figure 6: Variation of dimensionless buckling load of multi-scale hybrid nanocomposite plates *vs.* volume fraction of clusters for SSSS and CCCC edge conditions by considering partially and fully agglomerated CNTs (b/h=30, P=2, w_r=0.2, V_F=0.2)

Finally, effect of various BCs is included while drawing the variation of dimensionless buckling load against mass fraction of CNTs in Fig. 7. Herein it can be seen that buckling load can be added once a higher mass fraction is used for nanotubes (stiffening effect). Moreover, it can be observed that simply supported plates can endure small critical loads. In reverse, structures with either free or clamped edge conditions are better candidates for more critical static conditions.

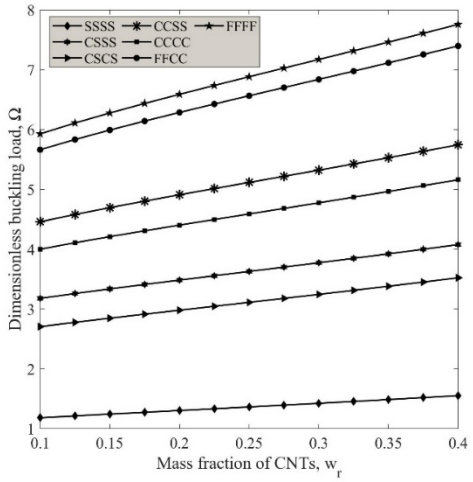

Figure 7: Effect of different boundary conditions on the variation of dimensionless buckling load of multi-scale hybrid nanocomposite square plates versus mass fraction of CNTs (a/h=30, P=2, V_F=0.2, μ=0.5, η=0.8)

5 Conclusions

In this manuscript, Hamilton's principle is mixed with a refined higher-order plate theory to reach the motion equations of a multi-scale hybrid nanocomposite plate. The nanocomposite, which is consisted of a polymer matrix, CFs and CNTs, is modeled utilizing Eshelby-Mori-Tanaka model incorporated with the rule of mixture. Influence of the nanofillers aggregation inside the inclusions is covered in this paper. The problem is solved on the basis of an analytical approach. Then, the non-dimensional form of results is presented for the sake of simplicity. Here, most important results are reviewed as follows:

- The buckling load can be amplified using higher mass fraction values for CNTs.
- Another way to intensify the critical buckling load once the CNTs are aggregated inside the inclusions is to employ a great volume fraction for clusters.
- Buckling load becomes smaller once the volume fraction of CNTs inside the clusters is increased.
- An increase in the value of CFs' volume fraction results in higher critical buckling loads.
- The structure can endure greater buckling loads once the CNTs are aggregated partially.

Conflicts of Interest: The authors declare that they have no conflicts of interest to report regarding the present study.

References

Aref, A. J.; Alampalli, S. (2001): Vibration characteristics of a fiber-reinforced polymer bridge superstructure. *Composite Structures*, vol. 52, pp. 467-474.

Aydogdu, M. (2007): Thermal buckling analysis of cross-ply laminated composite beams with general boundary conditions. *Composites Science and Technology*, vol. 67, pp. 1096-1104.

Aydogdu, M. (2009): A new shear deformation theory for laminated composite plates. *Composite Structures*, vol. 89, pp. 94-101.

Ćetković, M.; Vuksanović, D. (2009): Bending, free vibrations and buckling of laminated composite and sandwich plates using a layerwise displacement model. *Composite Structures*, vol. 88, pp. 219-227.

Chai, G. B.; Yap, C. W. (2008): Coupling effects in bending, buckling and free vibration of generally laminated composite beams. *Composites Science and Technology*, vol. 68, pp. 1664-1670.

Ebrahimi, F.; Farazmandnia, N. (2018): Thermal buckling analysis of functionally graded carbon nanotube-reinforced composite sandwich beams. *Steel and Composite Structures*, vol. 27, pp. 149-159.

Ebrahimi, F.; Habibi, S. (2017): Low-velocity impact response of laminated FG-CNT reinforced composite plates in thermal environment. *Advances in Nano Research*, vol. 5, pp. 69-97.

Ebrahimi, F.; Habibi, S. (2018): Nonlinear eccentric low-velocity impact response of a polymer-carbon nanotube-fiber multiscale nanocomposite plate resting on elastic foundations in hygrothermal environments. *Mechanics of Advanced Materials and Structures*, vol. 25, pp. 425-438.

Fazzolari, F. A.; Carrera, E. (2011): Advanced variable kinematics Ritz and Galerkin formulations for accurate buckling and vibration analysis of anisotropic laminated composite plates. *Composite Structures*, vol. 94, pp. 50-67.

Ferreira, A.; Roque, C.; Jorge, R. (2005): Free vibration analysis of symmetric laminated composite plates by FSDT and radial basis functions. *Computer Methods in Applied Mechanics and Engineering*, vol. 194, pp. 4265-4278.

García-Macías, E.; Rodríguez-Tembleque, L.; Castro-Triguero, R.; Sáez, A. (2017): Eshelby-Mori-Tanaka approach for post-buckling analysis of axially compressed functionally graded CNT/polymer composite cylindrical panels. *Composites Part B: Engineering*, vol. 128, pp. 208-224.

García-Macías, E.; Rodriguez-Tembleque, L.; Sáez, A. (2018): Bending and free vibration analysis of functionally graded graphene *vs.* carbon nanotube reinforced composite plates. *Composite Structures*, vol. 186, pp. 123-138.

Ghorbanpour Arani, A.; BabaAkbar Zarei, H.; Eskandari, M.; Pourmousa, P. (2017): Vibration behavior of visco-elastically coupled sandwich beams with magnetorheological core and three-phase carbon nanotubes/fiber/polymer composite facesheets subjected to external magnetic field. *Journal of Sandwich Structures & Materials*, 1099636217743177.

He, X.; Rafiee, M.; Mareishi, S.; Liew, K. (2015): Large amplitude vibration of fractionally damped viscoelastic CNTs/fiber/polymer multiscale composite beams. *Composite Structures*, vol. 131, pp. 1111-1123.

Heshmati, M.; Yas, M.; Daneshmand, F. (2015): A comprehensive study on the vibrational behavior of CNT-reinforced composite beams. *Composite Structures*, vol. 125, pp. 434-448.

Jam, J.; Kiani, Y. (2015): Low velocity impact response of functionally graded carbon nanotube reinforced composite beams in thermal environment. *Composite Structures*, vol. 132, pp. 35-43.

Ke, L. L.; Yang, J.; Kitipornchai, S. (2010): Nonlinear free vibration of functionally graded carbon nanotube-reinforced composite beams. *Composite Structures*, vol. 92, pp. 676-683.

Lei, Z.; Zhang, L.; Liew, K. (2015): Free vibration analysis of laminated FG-CNT reinforced composite rectangular plates using the kp-Ritz method. *Composite Structures*, vol. 127, pp. 245-259.

Lei, Z.; Zhang, L.; Liew, K. (2016): Parametric analysis of frequency of rotating laminated CNT reinforced functionally graded cylindrical panels. *Composites Part B: Engineering*, vol. 90, pp. 251-266.

Mareishi, S.; Rafiee, M.; He, X.; Liwe, K. (2014): Nonlinear free vibration, postbuckling and nonlinear static deflection of piezoelectric fiber-reinforced laminated composite beams. *Composites Part B: Engineering*, vol. 59, pp. 123-132.

Matsunaga, H. (2007): Vibration and buckling of cross-ply laminated composite circular cylindrical shells according to a global higher-order theory. *International Journal of Mechanical Sciences*, vol. 49, pp. 1060-1075.

Patel, B.; Ganapathi, M.; Makhecha, D. (2002): Hygrothermal effects on the structural behaviour of thick composite laminates using higher-order theory. *Composite Structures*, vol. 56, pp. 25-34.

Phung-Van, P.; Abdel-Wahab, M.; Liew, K. M.; Bordas, S. P. A.; Nguyen-Xuan, H. (2015): Isogeometric analysis of functionally graded carbon nanotube-reinforced composite plates using higher-order shear deformation theory. *Composite Structures*, vol. 123, pp. 137-149.

Rafiee, M.; Liu, X. F.; He, X. Q.; Kitipornchai, S. (2014): Geometrically nonlinear free vibration of shear deformable piezoelectric carbon nanotube/fiber/polymer multiscale laminated composite plates. *Journal of Sound and Vibration*, vol. 333, pp. 3236-3251.

Rafiee, M.; Nitzsche, F.; Labrosse, M. (2016): Rotating nanocomposite thin-walled beams undergoing large deformation. *Composite Structures*, vol. 150, pp. 191-199.

Rodrigues, J.; Roque, C.; Ferreira, A.; Carrera, E.; Cinefra, M. (2011): Radial basis functions-finite differences collocation and a Unified Formulation for bending, vibration and buckling analysis of laminated plates, according to Murakami's zig-zag theory. *Composite Structures*, vol. 93, no. 7, pp. 1613-1620.

Roy, T.; Chakraborty, D. (2009): Optimal vibration control of smart fiber reinforced composite shell structures using improved genetic algorithm. *Journal of Sound and Vibration*, vol. 319, pp. 15-40.

Sepahvand, K. (2016): Spectral stochastic finite element vibration analysis of fiber-reinforced composites with random fiber orientation. *Composite Structures*, vol. 145, pp. 119-128.

Shen, H. S.; Xiang, Y. (2014): Postbuckling of axially compressed nanotube-reinforced composite cylindrical panels resting on elastic foundations in thermal environments. *Composites Part B: Engineering*, vol. 67, pp. 50-61.

Shi, D. L.; Feng, X. Q.; Huang, Y. Y.; Hwang, K. C.; Gao, H. (2004): The effect of nanotube waviness and agglomeration on the elastic property of carbon nanotube-reinforced composites. *Journal of Engineering Materials and Technology*, vol. 126, no. 3, pp. 250-257.

Song, M.; Kitipornchai, S.; Yang, J. (2017): Free and forced vibrations of functionally graded polymer composite plates reinforced with graphene nanoplatelets. *Composite Structures*, vol. 159, pp. 579-588.

Song, M.; Yang, J.; Kitipornchai, S. (2018): Bending and buckling analyses of functionally graded polymer composite plates reinforced with graphene nanoplatelets. *Composites Part B: Engineering*, vol. 134, pp. 106-113.

Song, Z.; Zhang, L.; Liew, K. (2016): Dynamic responses of CNT reinforced composite plates subjected to impact loading. *Composites Part B: Engineering*, vol. 99, pp. 154-161.

Thai, C. H.; Ferreira, A. J. M.; Bordas, S. P. A.; Rabczuk, T.; Nguyenxuan, H. (2014): Isogeometric analysis of laminated composite and sandwich plates using a new inverse trigonometric shear deformation theory. *European Journal of Mechanics-A/Solids*, vol. 43, pp. 89-108.

Tita, V.; Carvalho, J. D.; Lirani, J. (2003): Theoretical and experimental dynamic analysis of fiber reinforced composite beams. *Journal of the Brazilian Society of Mechanical Sciences and Engineering*, vol. 25, pp. 306-310.

Wang, J.; Liew, K.; Tan, M.; Rajendran, S. (2002): Analysis of rectangular laminated composite plates via FSDT meshless method. *International Journal of Mechanical Sciences*, vol. 44, pp. 1275-1293.

Wang, L.; Hu, H. (2005): Flexural wave propagation in single-walled carbon nanotubes. *Physical Review B*, vol. 71, pp. 195412.

Wattanasakulpong, N.; Chaikittiratana, A. (2015): Exact solutions for static and dynamic analyses of carbon nanotube-reinforced composite plates with Pasternak elastic foundation. *Applied Mathematical Modelling*, vol. 39, pp. 5459-5472.

Yu, T.; Yin, S.; Bui, T. Q.; Xia, S.; Tanaka, S. et al. (2016): NURBS-based isogeometric analysis of buckling and free vibration problems for laminated composites plates with complicated cutouts using a new simple FSDT theory and level set method. *Thin-Walled Structures*, vol. 101, pp. 141-156.

Zenkour, A. (2004): Buckling of fiber-reinforced viscoelastic composite plates using various plate theories. *Journal of Engineering Mathematics*, vol. 50, pp. 75-93.

Zenkour, A.; Fares, M. (2001): Bending, buckling and free vibration of non-homogeneous composite laminated cylindrical shells using a refined first-order theory. *Composites Part B: Engineering*, vol. 32, pp. 237-247.

Zhu, P.; Lei, Z. X.; Lieu, K. M. (2012): Static and free vibration analyses of carbon nanotube-reinforced composite plates using finite element method with first order shear deformation plate theory. *Composite Structures*, vol. 94, no. 4, pp. 1450-1460.